High-Temperature Materials

SCIEPublish

Review

# Powder-Based Additive Manufacturing of $Ti_2AlNb$ Alloys: A Review of Processes, Microstructure and Mechanical Properties

**Ping Liu [1], Zhihao Zhu [2,*] and Liang Jia [2]**

[1] School of Materials Science and Engineering, Xi'an University of Technology, Xi'an 710074, China; liuping18709@163.com (P.L.)

[2] State Key Laboratory of Porous Metal Materials, Northwest Institute for Non-Ferrous Metal Research, Xi'an 710016, China; jialiang_nin@126.com (L.J.)

* Corresponding author. E-mail: zhuzhihaonin@163.com (Z.Z.)

Received: 10 April 2026; Revised: 20 April 2026; Accepted: 19 May 2026; Available online: 28 May 2026

**ABSTRACT:** $Ti_2AlNb$ alloy, a new generation of low-density titanium aluminide intermetallic compound, possesses excellent high-temperature strength, creep resistance, and moderate density, making it a promising candidate for high-temperature aerospace structural components. Powder-based additive manufacturing technology provides an effective approach for fabricating high-performance $Ti_2AlNb$ components, featuring high design freedom, efficient forming, and a controllable microstructure. This paper systematically reviews the research progress of powder-based additive manufacturing of $Ti_2AlNb$ alloys, focusing on three mainstream powder-based processes, including Selective Laser Melting (SLM), Selective Electron Beam Melting (SEBM), and Direct Laser Deposition (DLD). The regulation effect of the extreme non-equilibrium thermal cycle during powder-based additive manufacturing on the alloy microstructure is analyzed, and the correlation between process parameters and mechanical properties of components is summarized. Meanwhile, the key challenges in this field are identified, such as the difficulty in completely eliminating typical forming defects, insufficient precision of microstructure regulation, and a lack of theoretical guidance for process optimization. Finally, combined with technological development trends, future research directions are prospected from the aspects of defect control, microstructure, and mechanical property regulation, as well as engineering application.

**Keywords:** $Ti_2AlNb$ alloy; Powder-based additive manufacturing; Microstructure; Mechanical properties

## 1. Introduction

$Ti_2AlNb$ alloy exhibits exceptional high-temperature specific strength, favorable high-temperature oxidation resistance, and outstanding creep resistance, showing broad application prospects in aerospace [1,2]. It is an ideal high-temperature-resistant lightweight metallic material for achieving lightweight and high-performance aircraft structures [3]. This alloy can stably maintain high strength and excellent creep resistance within the high-temperature range of 650–900 °C. Meanwhile, its density is only 5.3–6.0 g/cm$^3$, approximately 40% lower than that of conventional nickel-based superalloys. Owing to its significantly

superior specific strength, which can effectively reduce aircraft structural weight and lower energy consumption [4,5]. Compared with existing high-temperature titanium alloys, $Ti_2AlNb$ alloy exhibits greater advantages in high-temperature strength and oxidation resistance, and is widely recognized as one of the most promising candidate materials for key hot-end complex components in advanced aero-engines [6]. Nevertheless, the ordered orthorhombic O-phase in $Ti_2AlNb$ alloy, while endowing it with excellent high-temperature properties, also introduces inherent challenges such as limited room-temperature slip systems, high deformation resistance, and a narrow hot-working window [7], posing significant difficulties for the forming and manufacturing of its components. When the traditional "casting and forging + machining" route is adopted to fabricate $Ti_2AlNb$ alloy components, it involves cumbersome process flows, high manufacturing costs, and extremely low material utilization. Moreover, defects such as cracking and deformation easily occur during processing, and the integrated forming of complex structural components is particularly difficult to achieve. This conventional approach can no longer satisfy the manufacturing requirements for complex components in the aerospace field [8–10].

Powder-based additive manufacturing, as an advanced technology, breaks through the bottlenecks of conventional manufacturing. Among various additive manufacturing technologies, the mainstream powder-based processes take powder as the raw material and fabricate three-dimensional solid components through layer-by-layer powder deposition, which is precisely guided by computer-aided design (CAD) digital models. This provides a breakthrough technical pathway for the high-performance fabrication of complex $Ti_2AlNb$ alloy components. This technology can not only increase material utilization to more than 80%, greatly shorten the manufacturing cycle, and reduce production costs, but also offer extremely high design freedom. By optimizing the microstructure of components through forming process control, it simultaneously improves their comprehensive mechanical properties, providing key manufacturing support for the upgrading and renewal of aerospace power systems and airframe structures [11–13]. At present, according to different powder delivery modes (powder feeding and powder spreading), powder-based additive manufacturing technologies can be divided into Directed Energy Deposition (DED) and Powder Bed Fusion (PBF) [14]. Research on $Ti_2AlNb$ alloy powder-based additive manufacturing has mainly focused on mainstream technical routes such as Selective Laser Melting (SLM) [6], Selective Electron Beam Melting (SEBM) [15], and Direct Laser Deposition (DLD) [16]. These powder-based additive manufacturing technologies exhibit unique advantages in the fabrication of extremely complex structures and rapid prototyping, and can precisely meet the forming requirements of core hot-end complex components in aero-engines.

In addition to powder-based additive manufacturing, wire-based processes, such as wire arc additive manufacturing (WAAM), have been explored for the fabrication of $Ti_2AlNb$ alloys. Recent studies have made preliminary progress using strategies such as single-wire preheating [17], dual-wire in-situ alloying [18,19], and hot-wire assistance [20]. While these attempts have yielded exploratory progress, wire-based process characteristics still bring inherent challenges such as microstructural inhomogeneity, obvious mechanical anisotropy, high hot-cracking sensitivity, and elemental segregation. These issues are closely associated with the ultra-high heat input and slow cooling rate inherent to the WAAM process, which easily trigger excessive grain coarsening and the precipitation of brittle, detrimental phases, leading to a relatively narrow processing window. For these reasons, the quality and performance consistency of as-fabricated components remain far below the demanding requirements of engineering applications. Against this background, powder-based additive manufacturing technologies, featuring smaller molten pool sizes, higher cooling rates, and greater flexibility in powder composition design, remain the core focus of this review and represent the most promising route for preparing high-performance $Ti_2AlNb$ alloys.

Although powder-based additive manufacturing offers distinct merits, its adoption in fabricating $Ti_2AlNb$ alloys still faces multiple key scientific and technical challenges. First, $Ti_2AlNb$ alloys show high sensitivity to thermal cycles, rendering metallurgical defects prone to form during layer-by-layer rapid

melting-solidification process. Precise regulation of processing parameters to mitigate defect generation is essential for guaranteeing component quality. Second, the rapid non-equilibrium solidification profoundly influences the size, morphology, and distribution of typical phases (e.g., O-phase and B2-phase). Since mechanical performance is intrinsically governed by microstructure, the inherent process–microstructure–property correlation requires further systematic exploration. Furthermore, well-designed post-process heat treatments are vital for tailoring phase constituents, enhancing microstructural stability, and improving overall mechanical performance, with relevant technical systems yet to be fully established and optimized.

To address these gaps, this paper systematically compares and analyzes the forming characteristics, microstructural evolution, and mechanical property differences among three mainstream powder-based additive manufacturing technologies—selective laser melting, selective electron beam melting, and direct laser deposition. It elucidates the regulatory mechanisms of thermal cycling characteristics from different processes on the phase composition, grain morphology, and mechanical properties of $Ti_2AlNb$ alloys, and further discusses their forming principles, process characteristics, microstructure formation mechanisms, mechanical property regulation strategies, and control methods for typical defects of each technology. Meanwhile, the key scientific and technical bottlenecks currently encountered in the powder-based additive manufacturing of $Ti_2AlNb$ alloy are identified, and the future research directions and development trends in this field are prospected. It is expected to provide references for the in-depth investigation, process optimization, and engineering application of powder-based additive manufacturing technologies for $Ti_2AlNb$ alloy components.

## 2. Composition and Phase Characteristics of $Ti_2AlNb$ Alloys

The chemical composition of $Ti_2AlNb$ alloys typically covers a range of Ti-(18–30 at.%) Al-(12.5–30 at.%) Nb. Researchers [21–23] have systematically explored the performance optimization of $Ti_2AlNb$ alloys, primarily via partial Nb substitution with Zr, Mo, Si, and other elements to further improve key mechanical properties such as strength, toughness, and oxidation resistance. Zhang et al. [24] investigated the tensile performance and fracture toughness of $Ti_2AlNb$ alloys with varying Al contents. They reported that reduced Al content appears to enhance fracture toughness while maintaining favorable strength and ductility. By comparison, higher Al content slightly improves strength but remarkably impairs ductility and fracture toughness. Appropriate Nb addition is beneficial to room-temperature ductility and high-temperature creep resistance. Germann et al. [25] adjusted Ti and Al contents and incorporated Mo, Si, and Zr as alloying elements. Their findings suggested that Nb doping can strengthen oxide scales and improve oxidation resistance; however, excessively high Nb content (above 15 at.%) weakens oxide scale adhesion and facilitates pore generation. Partial replacement of Nb with Zr, Mo, Si can effectively optimize creep performance without compromising ductility and yield strength. B enables grain refinement and enhances yield strength and room-temperature plasticity, though it may reduce ultimate tensile strength and elongation. Elements such as W, Ta, and Fe exhibit varying degrees of positive effects on strength, toughness, and creep resistance. While V boosts room-temperature ductility, it may degrade strength and oxidation resistance. By comprehensively comparing the composition–performance relationships of various $Ti_2AlNb$ systems, the Ti–22Al–25Nb alloy exhibits the most balanced mechanical properties, a stable microstructure, a mature manufacturing process, and reliable engineering applicability. Compared with other component ratios, it avoids the unilateral performance defects caused by excessive or insufficient single-element content and therefore becomes the most widely adopted and commercially mature composition for high-temperature aero-engine components.

The microstructure of $Ti_2AlNb$ alloys mainly comprises orthorhombic O-phase, body-centered cubic β/B2 phase, and hexagonal close-packed $\alpha_2$ phase. The morphology, distribution, and volume fraction of these phases largely determine the mechanical properties of the alloy. The β/B2 phase forms the continuous matrix and structural skeleton of the alloy. Featuring numerous slip systems, β and B2 phases primarily

accommodation strain during plastic deformation [2]. Nevertheless, ordering reduces atomic mobility, which may limit the overall ductility of the alloy. The $\alpha_2$ phase possesses an ordered hexagonal close-packed structure (similar to $Ti_3Al$) and serves as a low-temperature stable phase, precipitating predominantly from the β/B2 phase at moderate and low temperatures. Due to the absence of effective twinning modes, it is generally recognized as a brittle phase, which can adversely affect alloy toughness [1]. In comparison, the O-phase features an ordered orthorhombic structure and acts as the primary strengthening phase of $Ti_2AlNb$ alloy. It delivers superior creep resistance, high-temperature stability, and strengthening effect [26]. The O-phase exhibits favorable crystallographic matching with the B2/β matrix, enabling the formation of low-energy coherent interfaces. Such interfaces effectively hinder dislocation movement and stabilize the microstructure morphology, making the O-phase an essential strengthening constituent in $Ti_2AlNb$ alloys.

## 3. Powder-Based Additive Manufacturing of $Ti_2AlNb$ Alloy

### *3.1. Directed Energy Deposition (DED) of $Ti_2AlNb$ Alloy*

DED utilizes a high-energy-density heat source to generate a local molten pool on the substrate surface, while synchronously feeding raw powder into the pool for melting and solidification. Near-net-shape components are directly fabricated through layer-by-layer deposition [27]. DED mainly refers to DLD, whose working principle is illustrated in Figure 1a [28]. The key of this process lies in the precise delivery of metal powder into the laser-induced molten pool via a coaxial nozzle, thus realizing additive manufacturing of parts through successive cladding and deposition [29]. Benefiting from the coaxial powder feeding characteristic, DLD exhibits distinct advantages over conventional powder-bed additive manufacturing: it is free from the constraints of a closed build chamber, enabling the direct fabrication of large-scale complex components such as aero-engine casings and blisks. Moreover, it can be applied to the local repair of in-service parts and the direct deposition of functional structures on curved 3D surfaces, significantly improving the flexibility of $Ti_2AlNb$ alloy components in design, fabrication, and remanufacturing [30,31]. Although DLD offers numerous merits, including high forming efficiency, suitability for large-scale component production, and the capability to deposit multi-material composites and functionally graded structures, it tends to generate considerable residual stress during the forming process, which can lead to defects such as deformation and even cracking in the fabricated parts.

During the DLD fabrication of $Ti_2AlNb$ alloys, core processing parameters, including scanning speed, laser power, and linear energy density, critically modulate the microstructure and mechanical performance of as-deposited alloys via regulating the molten pool's thermal history and solidification behavior. In general, a higher scanning speed shortens laser-material interaction time, accelerating molten pool cooling and increasing the temperature gradient [13]. This contributes to grain refinement [32] and mitigates elemental segregation, facilitating the formation of uniform, fine acicular O-phase microstructures. However, excessively rapid solidification may induce microcracks in such ordered intermetallic systems and accumulate substantial residual stress owing to sharp temperature gradient variations [33]. As a comprehensive indicator of laser power and scanning speed, linear energy density serves as a key parameter governing the deposition quality, microstructure, and properties of $Ti_2AlNb$ alloys. Insufficient linear energy density prevents full melting of high-melting-point $Ti_2AlNb$ powder, leading to incomplete melting and easily inducing defects such as lack of fusion and porosity, reducing component densification and deteriorating high-temperature mechanical properties. In contrast, excessively elevated linear energy density enlarges the molten pool and causes significant thermal accumulation, resulting in grain coarsening, unbalanced phase constituents, and increased residual stress; in extreme cases, component deformation and cracking may occur. Accordingly, systematic optimization of DLD processing parameters is essential for fabricating complex $Ti_2AlNb$ alloy components to achieve a rational balance between energy input and

cooling rate. On the basis of guaranteed forming densification, precise regulation of the precipitation behavior of the B2 matrix and O-phase enables the acquisition of optimized as-deposited microstructure with excellent high-temperature strength, moderate ductility and improved crack propagation resistance. This can satisfy the requirements for long-term stable service of aero-engine high-temperature components under harsh service conditions.

### *3.2. Powder Bed Fusion (PBF) of $Ti_2AlNb$ Alloy*

PBF begins by uniformly spreading a thin powder layer on the building platform, then utilizes a high-energy beam (laser or electron beam) to selectively scan and melt powder feedstock in accordance with sliced cross-sectional data acquired from 3D digital models. Once a single layer is finished, a new layer of powder is deposited, and the foregoing procedures are repeated. Through this layer-by-layer stacking, a dense component is finally fabricated [34]. The PBF process mainly includes two categories: SLM and SEBM, whose schematic diagrams are shown in Figure 1 [29,35].

SLM employs a high-power-density laser beam [36] as the heat source and fabricates $Ti_2AlNb$ alloy components via layer-by-layer melting and high-precision forming under the protection of an inert atmosphere such as argon. Benefiting from the fine, focused laser spot and ultra-thin powder-spreading layer thickness, this process enables highly concentrated energy input and precise control over the forming procedure. It can integrally manufacture complex internal flow channels, topologically lightweight structures, thin-walled curved surfaces, and other features that are difficult to produce using conventional processing methods, yielding components with high dimensional accuracy and excellent surface quality [27]. Particularly importantly, the unique rapid melting and solidification behavior inherent to SLM promotes the formation of a fine and uniform microstructure in $Ti_2AlNb$ alloy and achieves a near-full dense forming state, thereby endowing it with excellent and stable comprehensive mechanical properties at both room and elevated temperatures [2]. Owing to the advantages of small molten pool size and high cooling rate, SLM is extremely suitable for fabricating small-sized $Ti_2AlNb$ components with high precision requirements and complex structures. However, its effective forming dimension is usually strictly limited by the build chamber volume of the powder bed [36].

SEBM uses a high-energy electron beam as the heat source, and the entire forming process is conducted in a vacuum environment. Due to the stronger penetration ability of electron beams into powder, SEBM exhibits more prominent technical advantages in the powder-based additive manufacturing of refractory alloy systems [37]. Meanwhile, this process is generally performed at a relatively high preheating temperature with a moderate cooling rate, which effectively reduces the residual stress generated during forming and thus decreases the cracking susceptibility of components, making it especially suitable for preparing the intrinsically brittle $Ti_2AlNb$ alloy [38]. $Ti_2AlNb$ alloy fabricated by SEBM exhibits strength equivalent to that of SLM counterparts, while its ductility and high-temperature service performance are more outstanding. In addition, SEBM is characterized by a high scanning speed, clean vacuum atmosphere, and low thermal stress during forming, which can further suppress deformation and microcrack initiation in components [39,40].

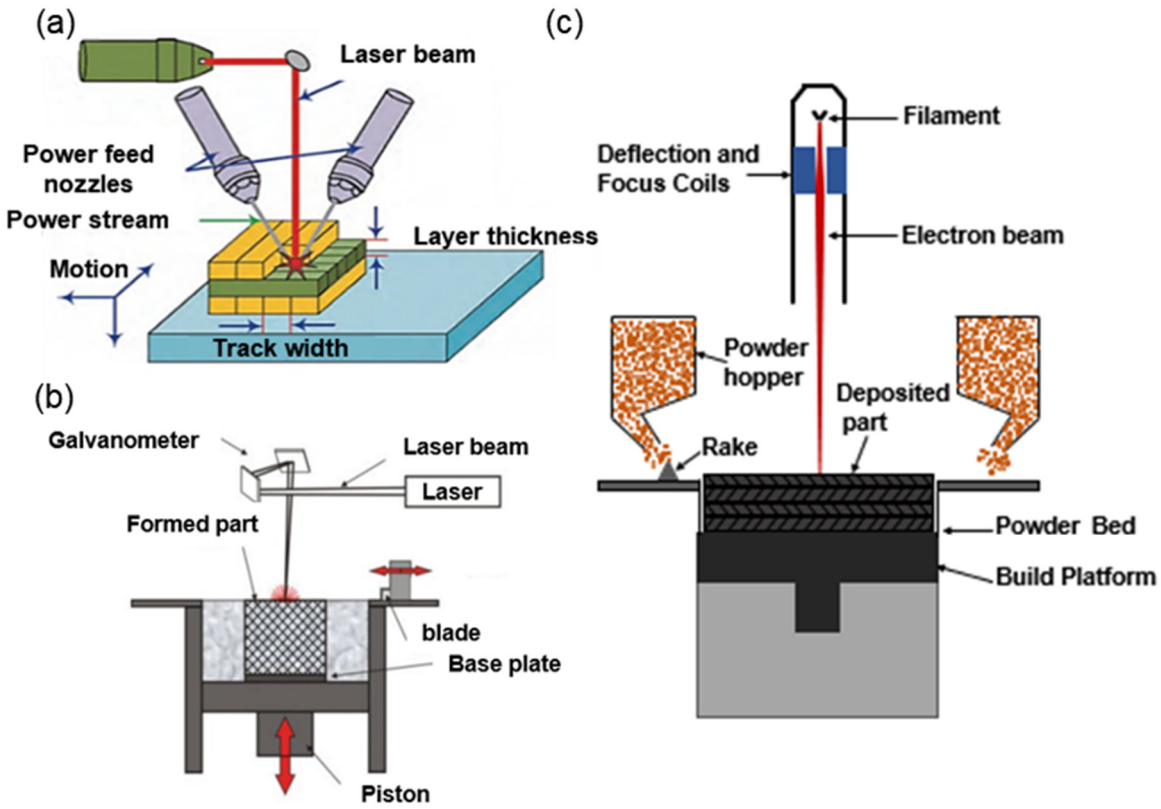


**Figure 1.** Schematic diagram of powder-based additive manufacturing technology [28,29]: (**a**) DLD, (**b**) SLM, and (**c**) SEBM. Modified based on Reference [35].

The extreme non-equilibrium thermal cycling environments inherent to different powder-based additive manufacturing processes exert a profound regulatory effect on the microstructure evolution and mechanical performance of $Ti_2AlNb$ intermetallic alloys, representing core scientific issues in the powder-based additive manufacturing of high-temperature structural materials. As a typical ordered intermetallic compound, $Ti_2AlNb$ alloys undergo complex solid-state phase transformations ($\beta \rightarrow \alpha_2 \rightarrow O$) during the heating and cooling cycles of powder-based additive manufacturing. The final phase composition, phase fraction, and distribution characteristics are not randomly generated but precisely controlled by two core thermal parameters: the cooling rate during solidification and subsequent cooling, and the preheating temperature of the substrate or powder bed (Figure 2a–c) [41]. These two parameters directly determine the thermodynamic driving force and kinetic rate of phase transformations, yielding distinct microstructural features in $Ti_2AlNb$ alloys fabricated by different powder-based additive manufacturing processes. This largely accounts for the evident differences in their mechanical properties. As demonstrated by electron backscatter diffraction (EBSD) phase distribution maps (Figure 2a–c), $Ti_2AlNb$ alloys fabricated by SEBM exhibit a typical hierarchical microstructure, consisting of a continuous β-phase (B2 structure, marked in green) as the matrix, with uniformly precipitated lath-like O-phase (orthorhombic structure, marked in red) within the β grains, accompanied by well-defined and coarse β grain boundaries. This unique microstructural characteristic is strongly governed by the thermal cycling characteristics of the SEBM process: SEBM employs high-temperature preheating of the powder bed at 600–1000 °C, which effectively reduces the temperature gradient and thermal stress during forming and extends the molten pool cooling duration. Such thermal conditions provide sufficient thermodynamic support for the stable retention of the β-phase and nucleation and growth of the O-phase. this microstructure, lath-like O-phase efficiently hinders dislocation movement, while the continuous β matrix maintains favorable deformability, establishing a sound microstructural foundation for the excellent high-temperature creep resistance and moderate room-

temperature ductility of SEBM-fabricated $Ti_2AlNb$ alloys. In comparison, $Ti_2AlNb$ alloys fabricated by SLM are dominated by a supersaturated β matrix (marked in green) with minimal O-phase content, and the microstructure is characterized by coarse columnar β grains spanning multiple deposited layers with clear and straight grain boundaries. The formation of this microstructure is attributed to the unique thermal cycling of the SLM process: SLM uses a high-energy-density laser beam (power density up to $10^6$ W/cm$^2$) to rapidly melt the powder, resulting in an ultra-high cooling rate (106–108 K/s) during solidification. This extreme non-equilibrium thermal condition significantly inhibits the solid-state phase transformation of β→$\alpha_2$→O, making the high-temperature β-phase (B2 structure) retained stably to room temperature, forming a supersaturated β matrix. The extremely low content of O-phase and the coarse columnar β grain structure led to the high room-temperature strength but poor ductility of SLM-fabricated $Ti_2AlNb$ alloys, which also makes the material prone to cracking during the forming process.

In contrast to both SEBM and SLM processes, the $Ti_2AlNb$ alloy fabricated by direct laser deposition (DLD) presents a refined triphase coexistence structure, consisting of β/B2 phase (marked in red, volume fraction 23.5%), $\alpha_2$ phase (marked in yellow, volume fraction 45.0%), and O-phase (marked in blue, volume fraction 31.7%). This distinct microstructural feature is an inevitable result of the moderate thermal cycling of the DLD process: DLD adopts a coaxial powder feeding mode, and the interaction between the laser beam and the powder forms a molten pool with moderate size and cooling rate ($10^3$–$10^5$ K/s); at the same time, the layer-by-layer cladding process leads to repeated remelting and reheating of the previously deposited layers, forming a multi-pass thermal cycle. This thermal environment avoids both the phase transformation inhibition and metastable phase retention caused by excessive cooling in SLM, and the excessive grain growth induced by high-temperature preheating in SEBM, thereby realizing the synergistic regulation of β/B2, $\alpha_2$, and O three phases, and forming a refined microstructure, which is conducive to the improvement of the strength and ductility matching of the alloy. The transmission electron microscopy (TEM) observations (Figure 2d–f) [42,43] further reveal the fine-scale microstructural characteristics and defect evolution of $Ti_2AlNb$ alloys fabricated by different powder-based additive manufacturing processes, which provide direct experimental evidence for the correlation between thermal cycling, microstructure, and mechanical properties. Specifically, the TEM bright-field image of the SEBM-fabricated sample (Figure 2d) shows that there are a large number of high-density dislocations in the β matrix, and these dislocations are pinned and entangled at the interface between the O-phase and the β matrix; the lath-like O-phase is uniformly embedded in the β matrix, forming a composite strengthening mechanism of dislocation strengthening and second-phase strengthening. As shown in Figure 2e, during the SLM process, the sub-grain boundaries formed by dislocation rearrangement serve as low-energy nucleation sites for the O-phase, promoting its directional growth along dislocation slip directions and generating a feathery bundle morphology. In contrast, $Ti_2AlNb$ alloys fabricated via DLD possess distinctly different dislocation configurations, mainly classified into two typical morphologies: curved and entangled dislocation loops, and oriented dislocation walls consisting of straight dislocations (Figure 2f). The coexistence of these two dislocation structures implies that the DLD alloy can activate more dislocation slip systems during deformation, delivering improved plastic deformability while retaining high strength.

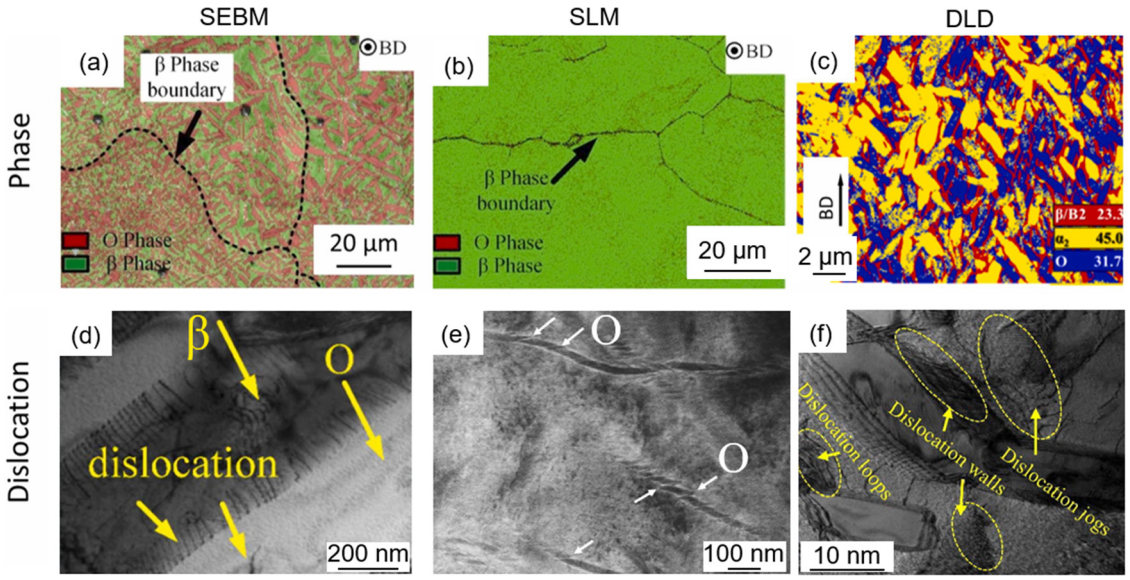


**Figure 2.** EBSD and TEM characterization of $Ti_2AlNb$ alloys fabricated by three powder-based additive manufacturing processes [41–43]: (**a**–**c**) phase distribution maps, and (**d**–**f**) dislocations in β matrix and O-phase laths.

Figure 3 systematically compares the room-temperature tensile properties of $Ti_2AlNb$ alloys fabricated via diverse manufacturing routes, including powder-based additive manufacturing, conventional forging, and powder metallurgy (PM) [44]. Data from the literature for comparison were also listed in Table 1. The results reveal distinct performance windows for different processing routes. Specifically, powder-based additive manufacturing of $Ti_2AlNb$ alloys (SLM, SEBM, LMD) presents a high-strength yet low ductility: the ultimate tensile strength (UTS) ranges from 900 to 1250 MPa, while the elongation is maintained at merely 2–8%. Among these processes, SEBM-fabricated samples achieve superior strength-ductility synergy. This improvement stems from the unique hierarchical β+O lath microstructure formed at high temperatures, which well balances fine subgrain strengthening and residual stress relaxation. By contrast, conventionally forged $Ti_2AlNb$ alloys deliver excellent comprehensive performance, with high strength (1050–1150 MPa) and exceptional ductility (8–16%). Such excellent properties benefit from intense thermomechanical deformation during forging, which refines grain structures, removes internal defects, and promotes microstructure homogenization. However, the industrial application of forged $Ti_2AlNb$ is significantly constrained by high cost, low material yield, and difficulty in net-shaping complex components. On the other hand, powder metallurgy (PM) routes, such as cold sintering (CS) and spark plasma sintering (SPS), generally result in relatively low UTS (300–950 MPa) and moderate ductility. This performance limitation primarily originates from inherent porosity and insufficient densification in PM-derived microstructures, which act as stress concentration centers and preferential crack initiation sites, seriously weakening the mechanical performance.

Collectively, this comparison results fully demonstrate that fabrication route dominates the microstructure, defects, and phase distribution, thereby determining the final mechanical performance of $Ti_2AlNb$ alloys. Each processing route has its own inherent merits and limitations: forging excels in comprehensive mechanical properties but lacks forming flexibility; powder metallurgy offers low cost but suffers from poor strength; and powder-based additive manufacturing offers unparalleled advantages for fabricating complex, customized components but is restricted by lower ductility compared with forged counterparts. Notably, powder-based additive manufacturing, in particular SEBM, shows considerable promise for producing high-performance, complex $Ti_2AlNb$ components that are not feasible via conventional routes. Future research could focus on process parameter optimization and rational post-heat treatments to enhance the ductility of additively manufactured alloys, reduce the performance disparity

relative to forged counterparts, and support the practical large-scale application of powder-based additive manufacturing $Ti_2AlNb$ alloys in aero-engine hot-end components.

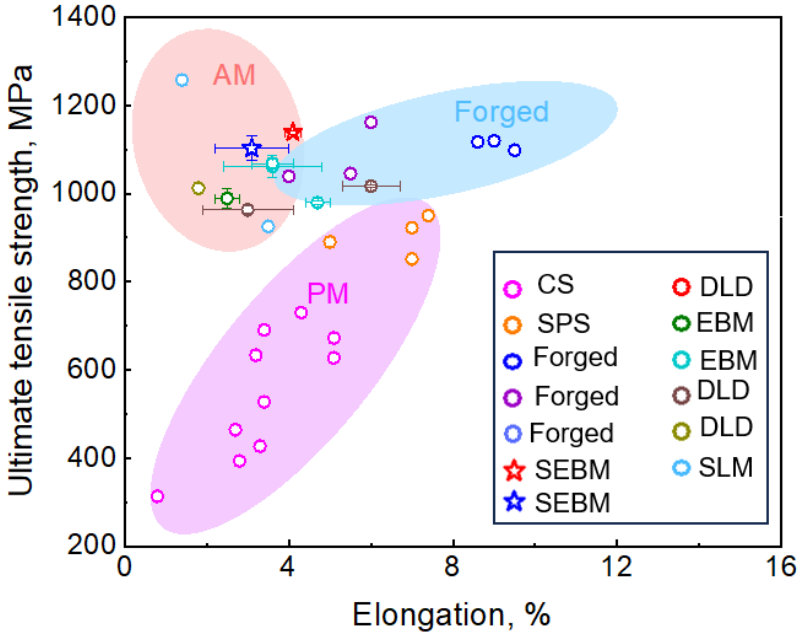


**Figure 3.** Comparison of room-temperature tensile properties (ultimate tensile strength *vs*. elongation) of $Ti_2AlNb$ alloys fabricated by additive manufacturing (AM), forging, and powder metallurgy (PM). SEBM, SLM, DLD for AM; forged for conventional forging; SPS, CS for PM. Modified based on Reference [44].

**Table 1.** Tensile properties of as-deposited $Ti_2AlNb$ at ambient temperature and 650 °C [44–53].

| Materials | Tensile Tests Temperature | Fabrication [a] | Tensile Properties [b] | | |
|---|---|---|---|---|---|
| | (°C) | | YS (MPa) | UTS (MPa) | EL (%) |
| Ti–22Al–25Nb | 25 | PM | 151 | 314 | 0.8 |
| Ti–22Al–25Nb | 25 | PM | 192 | 393 | 2.8 |
| Ti–22Al–25Nb | 25 | PM | 318 | 427 | 3.3 |
| Ti–22Al–25Nb | 25 | PM | 440 | 527 | 3.4 |
| Ti–22Al–25Nb | 25 | PM | 544 | 672 | 5.1 |
| Ti–22Al–25Nb | 25 | PM | 607 | 730 | 4.3 |
| Ti–22Al–25Nb | 25 | PM | 353 | 465 | 2.7 |
| Ti–22Al–25Nb | 25 | PM | 525 | 633 | 3.2 |
| Ti–22Al–25Nb | 25 | PM | 544 | 627 | 5.1 |
| Ti–22Al–25Nb | 25 | PM | 586 | 690 | 3.4 |
| Ti–22Al–25Nb | 25 | SPS | 865 | 922 | 7 |
| Ti–22Al–25Nb | 25 | SPS | 868 | 950 | 7.4 |
| Ti–22Al–25Nb | 25 | SPS | 809 | 890 | 5 |
| Ti–22Al–25Nb | 25 | SPS | 849 | 852 | 7 |
| Ti–22Al–25Nb | 25 | Forged | 1004 | 1117 | 8.6 |
| Ti–22Al–25Nb | 25 | Forged | 1001 | 1098 | 9.5 |
| Ti–22Al–25Nb | 25 | Forged | 1007 | 1119 | 9.0 |
| Ti–22Al–25Nb | 25 | Forged | 1076 | 1162 | 6.0 |
| Ti–22Al–25Nb | 25 | Forged | 974 | 1045 | 5.5 |
| Ti–22Al–25Nb | 25 | Forged | 956 | 1039 | 4.0 |
| Ti–22Al–25Nb | 25 | SEBM | 943 ± 20 | 989 ± 22 | 2.5 ± 0.3 |
| Ti–22Al–25Nb | 25 | SEBM | - | 1068 ± 12 | 3.6 ± 0.5 |
| Ti–22Al–25Nb | 25 | SEBM | - | 979 ± 6 | 7.3 ± 0.6 |
| Ti–22Al–25Nb | 25 | SEBM | 991 ± 4 | 1139 ± 6 | 4.1 ± 0.2 |

| | | | | | |
|---|---|---|---|---|---|
| Ti–22Al–25Nb | 25 | DLD | - | 1017 ± 13 | 6 ± 0.7 |
| Ti–22Al–25Nb | 25 | DLD | - | 963 ± 8 | 3 ± 1.1 |
| Ti–22Al–25Nb | 25 | DLD | - | 971 ± 36 | 1.9 ± 0.7 |
| Ti–22Al–25Nb | 25 | DLD | - | 966 ± 7 | 4.5 ± 0.5 |
| Ti–22Al–25Nb | 25 | DLD | - | 1012 | 1.8 |
| Ti–22Al–25Nb | 25 | SLM | 932 ± 18 | 947 ± 13 | 15 ± 1 |
| Ti–22Al–25Nb | 25 | SLM | 990 ± 15 | 1005 ± 14 | 13 ± 1 |
| Ti–22Al–25Nb | 25 | SLM | 1051 ± 12 | 1066 ± 18 | 12 ± 1 |
| Ti–22Al–25Nb | 25 | SLM | 1080 ± 14 | 1099 ± 11 | 11 ± 1 |
| Ti–22Al–25Nb | 650 | PM | 225 | 353 | 6.8 |
| Ti–22Al–25Nb | 650 | PM | 342 | 431 | 7.5 |
| Ti–22Al–25Nb | 650 | PM | 506 | 625 | 7.2 |
| Ti–22Al–25Nb | 650 | PM | 486 | 608 | 7.9 |
| Ti–22Al–25Nb | 650 | PM | 386 | 469 | 5.7 |
| Ti–22Al–25Nb | 650 | PM | 508 | 621 | 7.4 |
| Ti–22Al–25Nb | 650 | PM | 536 | 645 | 7.0 |
| Ti–22Al–25Nb | 650 | Forged | 863 | 976 | 18.3 |
| Ti–22Al–25Nb | 650 | Forged | 837 | 923 | 14.7 |
| Ti–22Al–25Nb | 650 | Forged | 796 | 882 | 12.5 |
| Ti–22Al–25Nb | 650 | SLM | - | 411 ± 29 | 0.4 ± 0.1 |
| Ti–22Al–25Nb | 650 | SLM | - | 364 ± 40 | 0.3 ± 0.1 |
| Ti–22Al–25Nb | 650 | SLM | - | 333 ± 36 | 0.3 ± 0.1 |
| Ti–22Al–25Nb | 650 | SLM | - | 321 ± 37 | 0.2 ± 0.1 |
| Ti–22Al–25Nb | 650 | SEBM | 741 ± 24 | 803 ± 30 | 3 ± 0.5 |

[a] PM, SPS, SLM, DLD, and EBM denote powder metallurgy, spark plasma sintering, selective laser melting, direct laser deposition, and selective electron beam melting, respectively. [b] YS, UTS, and EL denote, respectively, tensile yield strength, ultimate tensile strength, and total elongation.

Compared with conventional forging and powder metallurgy routes, powder-based additive manufacturing technologies offer unique technical advantages for industrial applications, including the integrated forming of complex structural components, shorter manufacturing cycles, higher material utilization, and greater adaptability to customized production and rapid manufacturing iteration. However, several practical challenges remain for industrial implementation, such as low forming efficiency, high equipment and raw material costs, limited process stability and reproducibility, as well as imperfect industrial specifications and quality certification systems. These differentiated advantages and constraints suggest that each manufacturing route has its suitable application scope and technical limitations. The current limitations of powder-based additive manufacturing may, to some extent, restrict its large-scale and standardized engineering applications, indicating that it cannot yet fully replace traditional processing methods in the mass production of $Ti_2AlNb$ alloy components.

## 4. Analysis of Typical Defects

### *4.1. Hot Cracking*

During the layer-by-layer deposition process of powder-based additive manufacturing of $Ti_2AlNb$ alloys, the material experiences repeated rapid melting and solidification cycles. This non-equilibrium thermal process can generate a steep temperature gradient inside the component, which in turn induces thermal stress that may accumulate progressively. When the accumulated thermal stress exceeds the tensile strength limit of the $Ti_2AlNb$ alloy, microcracks initiate inside the component. These initial microcracks do not disappear spontaneously; instead, during subsequent thermal cycles in powder-based additive manufacturing and under applied loads after forming, they propagate and extend continuously, eventually

forming macroscopic thermal cracks visible to the naked eye. This severely compromises the structural integrity and mechanical properties of the component [54], as shown in Figure 4a [41].

The hot cracking susceptibility of the $Ti_2AlNb$ alloy is not solely intrinsic; it is influenced by multiple factors. Among them, the setting of powder-based additive manufacturing process parameters and the substrate preheating temperature are among the most critical influencing factors. In addition, the geometry of the component and the protective atmosphere during forming also affect the formation of thermal cracks. At present, several strategies have been developed to control thermal cracks during the powder-based additive manufacturing of $Ti_2AlNb$ alloy, mainly including optimization of the base material composition, precise regulation of powder-based additive manufacturing process parameters, and preheating treatment before forming [55]. Taking laser additive manufacturing as an example, within a suitable process window, appropriately increasing the laser power or reducing the scanning speed can increase the energy input and the molten pool residence time, and reduce the temperature gradient within the component, thereby decreasing the number of cracks and suppressing the material's cracking tendency. The comparative experimental results from SLM-fabricated Ti–22Al–25Nb alloys illustrate such parameter-dependent performance variation [56]. Excessively low scanning speed (0.4 m/s) induces excessively high energy density, generating abundant pore defects and resulting in moderate mechanical properties (YS of 933 MPa, UTS of 939 MPa, EL of 12%). In comparison, excessively high scanning speed (1.2 m/s) produces insufficient energy density of only 32.41 J/mm$^3$, which triggers severe lack-of-fusion defects and causes more significant performance deterioration (YS of 862 MPa, UTS of 898 MPa, EL of 4%). In contrast, the medium scanning speed range of 0.6–0.8 m/s provides matched energy input, effectively suppressing internal defects and achieving a relative density above 99%. This optimal parameter window exhibits tunable performance characteristics: a relatively low speed of 0.6 m/s favors ductility, with a maximum elongation of 15%, whereas a slightly higher speed of 0.8 m/s improves strength, delivering YS of 982 MPa and UTS of 989 MPa. Such performance differences suggest that rational scanning speed can help achieve superior strength–ductility synergy [56]. Furthermore, substrate preheating serves as a useful complementary strategy. It reduces the thermal gradient during forming, alleviates rapid accumulation of thermal stress, and restrains the initiation and propagation of thermal cracks, thereby further improving the overall forming quality of the component.

### *4.2. Lack of Fusion*

Lack of fusion is another typical processing defect in the powder-based additive manufacturing of $Ti_2AlNb$ alloy. It typically exhibits a flat or elongated morphology, mainly distributed along the interfaces between adjacent melt tracks or interlayer boundaries of successive deposited layers. The defect edges are generally smooth, and unmelted residual particles can often be observed inside the defect. Such defects severely break the metallurgical bonding continuity inside the component, causing a drastic deterioration of its mechanical properties and even premature service failure, as shown in Figure 4b [4]. The essential cause of lack of fusion defects is insufficient energy input during powder-based additive manufacturing, which fails to fully melt the deposited material, or inappropriate scanning strategies that lead to poor overlapping between adjacent melt tracks and deposited layers, failing to form effective metallurgical bonding.

Based on the forming characteristics of $Ti_2AlNb$ alloy and the inherent features of powder-based additive manufacturing processes, the formation of lack-of-fusion defects can be mainly attributed to the following three typical scenarios: First, an excessively low linear energy density, indicating that the energy input from the heat source is inadequate to endow the molten pool with sufficient volume and superheat temperature. This fails to achieve full melting of the current deposited layer and the surface metal of the previous layer, causing cold bonding between adjacent layers and eventually resulting in interlayer lack of fusion. Second, an overlarge hatch spacing results in insufficient overlap between adjacent melt tracks. Unmelted regions remain in the gaps between tracks, forming inter-track lack of fusion. Third, a powder

layer thickness exceeding the effective penetration depth of the heat source, which leaves the underlying substrate material partially unmelted. This phenomenon is more pronounced in SEBM and high-deposition-rate DLD processes, and exhibits a high tendency to induce interlayer lack-of-fusion defects [57].

Unlike other metallurgical defects, such as hot cracks and porosity, once formed, lack-of-fusion defects are more difficult to eliminate through conventional post-processing methods. Hot isostatic pressing (HIP), although a commonly used and effective post-processing technique, has shown certain success in improving the densification of additively manufactured components and mitigating some metallurgical defects. However, its effectiveness against lack-of-fusion defects remains limited. HIP can only achieve localized and partial densification, struggling to repair the incomplete metallurgical bonding interface in the unfused region or eliminate the inherent interlayer and inter-track interfacial gaps. Therefore, the prevention and active control of lack-of-fusion defects should primarily rely on targeted strategies during the forming process. Current mainstream control measures include: appropriately matching laser or electron beam power with scanning speed to achieve a suitable linear energy density and ensure complete melting of the material; optimizing hatch spacing and powder layer thickness to ensure adequate overlap between adjacent melt tracks and deposited layers; and integrating real-time molten pool monitoring systems to identify, provide feedback on, and regulate abnormal conditions during the forming process, thereby adjusting process parameters dynamically, and fundamentally reducing the formation of lack-of-fusion defects.

### *4.3. Porosity*

Porosity is a common metallurgical defect in powder-based additive manufacturing of $Ti_2AlNb$ alloys. It can reduce and undermine the densification of the internal microstructure, compromising strength, toughness, and fatigue properties, and may even induce other secondary defects in severe cases, as shown in Figure 4c [4,58]. Based on their formation mechanisms, porosity can be categorized into two categories: metallurgical porosity and process-induced porosity. These two types differ in their origins and morphological characteristics, but both can adversely affect forming quality and service performance.

During the rapid forming process of powder-based additive manufacturing, the molten pool is at a high temperature and in an unstable state. The drastic thermal fluctuations induced by rapid melting and solidification can trigger severe fluid flow instability of the molten pool, resulting in violent fluctuations on the molten pool surface. In this case, the inert gas (such as argon) used to protect the molten pool during forming is easily entrapped by the flowing liquid metal and eventually encapsulated inside the component after solidification, forming process-induced porosity. Simultaneously, under high-temperature conditions, gases such as hydrogen and nitrogen from the ambient atmosphere and residual gases in the fabrication system dissolve extensively into the high-temperature molten pool. Given the extremely high cooling rate during powder-based additive manufacturing of the $Ti_2AlNb$ alloy, the solubility of gases in the metal decreases rapidly as the molten pool temperature drops sharply. These supersaturated gases cannot precipitate and escape from the solidification interface in time, and are ultimately trapped by the solidified metal, forming metallurgical porosity [55].

Relevant research results show that the formation of porosity in the powder-based additive manufacturing of $Ti_2AlNb$ alloy is associated with the keyhole depression phenomenon and the setting of powder-based additive manufacturing process parameters. Core process parameters, including laser power, scanning speed, and powder layer thickness, directly regulate the temperature field distribution, solidification rate, and melt flow behavior of the molten pool, thereby determining the keyhole stability, melt flow pattern, and bubble escape window size. These parameters ultimately play a decisive role in the type, quantity, size, and spatial distribution of pores. Therefore, establishing and optimizing the process window of powder-based additive manufacturing through systematic experimental investigations, mitigating keyhole fluctuation and collapse, prolonging bubble escape time, and facilitating sufficient precipitation and escape of supersaturated gases in the molten pool constitutes a key technical approach to

reduce porosity defects and enhance the densification of additively manufactured $Ti_2AlNb$ alloy components [55].

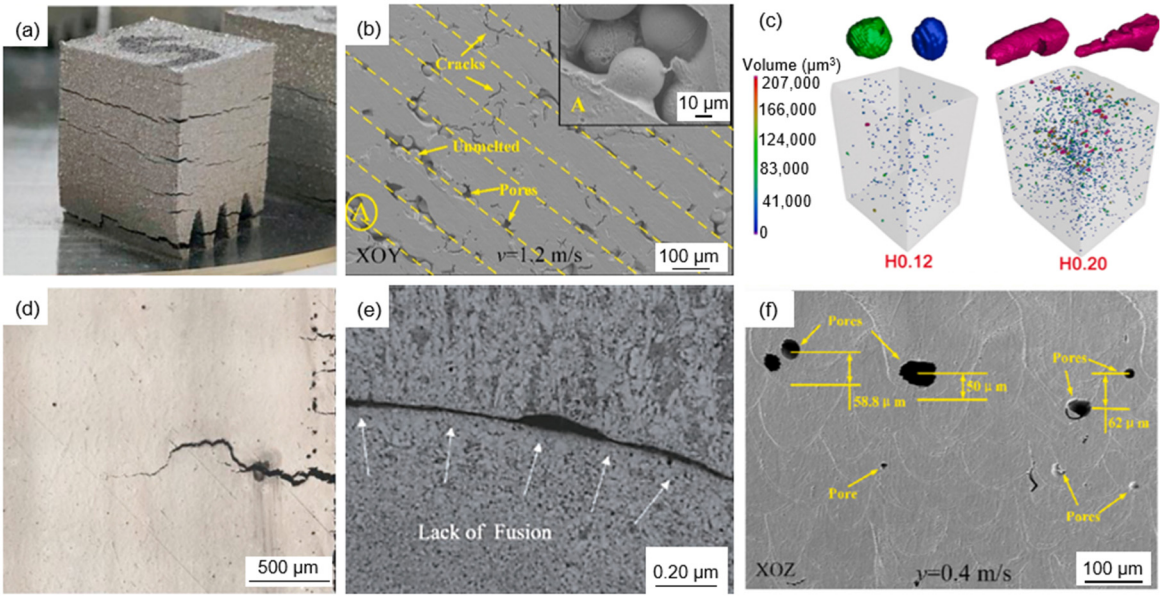


**Figure 4.** Typical metallurgical defects in the additive-manufactured $Ti_2AlNb$ alloys [4,41,57]: (**a**,**d**) Hot Cracking, (**b**,**e**) Lack of Fusion, and (**c**,**f**) Porosity.

## 5. Conclusions

To objectively and critically clarify the potential for actual application and the core technical bottlenecks of the $Ti_2AlNb$ alloy, this study focuses on the regulatory effect of powder-based additive manufacturing on the alloy's microstructure and mechanical properties. Based on a comprehensive analysis of experimental results and related mechanisms, the key conclusions and future development directions of additively manufactured $Ti_2AlNb$ alloy are summarized as follows:

(1) Powder-based additive manufacturing can effectively address $Ti_2AlNb$'s brittleness and narrow processing window. Optimized SLM, SEBM, and DLD can achieve >99% densification, with some studies reporting UTS >1100 MPa—comparable to, or even exceeding that of, conventionally manufactured components. While microstructure evolution has been clarified, only a preliminary process-structure-property correlation has been established, which may be insufficient for industrial-scale performance control.

(2) Despite certain progress in powder-based additive manufacturing of $Ti_2AlNb$, severe and unresolved critical bottlenecks persist: hot cracking, porosity and lack of fusion remain extremely hard to eliminate (formation mechanisms and process correlation remain unfully clarified); microstructure control is highly imprecise (inhomogeneous phases and grains, with anisotropy impact still requiring further study); process optimization excessively relies on experience, with serious residual stress and fatigue data gaps severely hindering precise performance regulation.

(3) The future development of powder-based additive manufacturing of $Ti_2AlNb$ alloys is expected to focus on phased technological breakthroughs and systematic industrialization. Key short-term priorities include elucidating critical defect mechanisms and developing targeted control strategies, realizing high-precision microstructure control, and establishing a robust quantitative process–microstructure–properties model. Long-term goals may involve developing intelligent, engineering-oriented technology, expanding advanced new powder-based additive manufacturing processes, optimizing alloy and processing, and furthering the application of $Ti_2AlNb$ alloys.

## Author Contributions

P.L.: Investigation, Validation, Writing—original draft, Writing—review & editing. Z.Z.: Conceptualization, Formal analysis, Writing—review & editing, Supervision, Funding acquisition. L.J.: Validation.

## Ethics Statement

Not applicable.

## Informed Consent Statement

Not applicable.

## Data Availability Statement

Data availability is not applicable to this article as no new data were created or analyzed in this study.

## Funding

This research was funded by the Key Research and Development Project of Shaanxi Province (No. 2025CY-YBXM-579, No. 2025CY-GJHX-17), the Research Project of Northwest Institute for Nonferrous Metal Research (No. 0601YK2520), the National Natural Science Foundation of China (No. 52304387), the Shaanxi Provincial Young Science and Technology Star Project under the Innovation Talent Promotion Program (No. 2025ZC-KJXX-95), and the Innovation Capability Support Program of Shaanxi (No. 2023-CX-TD-54).

## Declaration of competing interest

The authors declare that they have no known competing financial interests or personal relationships that could have appeared to influence the work reported in this paper.

## References

1. Hu JX, He ZH, Cong ZR, Liu YZ, Li S, Wang YJ, et al. The structure and applications in the materials field of $Ti_2AlNb$ alloy: A review. *Rev. Mater. Res.* **2026**, *2*, 100131. DOI:10.1016/j.revmat.2025.100131
2. Hu R, Zhang KW, Zou H, Gao ZT, Luo X, Liu XX, et al. Research progress on $Ti_2AlNb$-based alloys and composites for aerospace applications. *J. Alloys Compd.* **2025**, *1021*, 179701. DOI:10.1016/j.jallcom.2025.179701
3. Wang JK, Ding ZJ, Wang B, Qin ZW, Wei BH, Hong XL, et al. Strain-field tailoring via reticular architectures for high-performance $Ti_2AlNb$ components. *J. Alloys Compd.* **2026**, *1058*, 187022. DOI:10.1016/j.jallcom.2026.187022
4. Liao JF, Fan AQ, Luo HJ, Du YL. Research progress of laser powder bed fusion of $Ti_2AlNb$-based alloys: Microstructure, defects and properties. *J. Mater. Res. Technol.* **2025**, *35*, 3393–3409. DOI:10.1016/j.jmrt.2025.02.037
5. Lin J, Sui XC, Cheng S, Wang GF, Li ZW. Precipitation mechanism of nano-size O phase in single B2 phase $Ti_2AlNb$ alloy. *Chin. J. Aeronaut.* **2025**, *38*, 103596. DOI:10.1016/j.cja.2025.103596
6. Man JY, Huang LH, He JJ, Yang HO, Lin X. Effect of heat treatment on microstructure and properties of $Ti_2AlNb$ alloy formed by selective laser melting. *J. Mater. Res. Technol.* **2024**, *33*, 2549–2559. DOI:10.1016/j.jmrt.2024.09.243
7. Li ZH, Guo BD, Wang D, Wang J, Li XL, Xue SB, et al. Improvement room and high temperature ductility by regulating O-phase lath structure for $Ti_2AlNb$ alloy. *J. Alloys Compd.* **2025**, *1039*, 183259. DOI:10.1016/j.jallcom.2025.183259
8. Goyal K, Sardana N. Phase stability and microstructural evolution of $Ti_2AlNb$ alloys—A review. *Mater. Today Proc.* **2021**, *41*, 951–968. DOI:10.1016/j.matpr.2020.10.925
9. Liu YJ, Yang XJ, Jiao WH. Enhancing high-temperature creep resistance of additively manufactured $Ti_2AlNb$ alloys via vacuum hot isostatic pressing-induced tailoring of coherent interfaces. *Vacuum* **2025**, *239*, 114392. DOI:10.1016/j.vacuum.2025.114392
10. Luo S, Li XB, Zhang X, Zhang CC, Tang JW, Yan WC, et al. Research progress on microstructural defects and regulation technologies of titanium alloys in laser additive manufacturing. *Int. J. Refract. Met. Hard Mater.* **2026**, *139*, 107803. DOI:10.1016/j.ijrmhm.2026.107803

11. Gardner L. Metal additive manufacturing in structural engineering—Review, advances, opportunities and outlook. *Structures* **2023**, *47*, 2178–2193. DOI:10.1016/j.istruc.2022.12.039
12. Das B, Sahoo N, Patel P, Ghosh A, Khan MA, Bhushan B, et al. Wire Arc Additive Manufacturing (WAAM): A comprehensive review of process, materials, modelling, artificial intelligence, and industrial applications. *J. Alloys Compd.* **2026**, *1058*, 186347. DOI:10.1016/j.jallcom.2026.186347
13. Zhou YH, Li WP, Wang DW, Zhang L, Ohara K, Shen J, et al. Selective laser melting enabled additive manufacturing of Ti–22Al–25Nb intermetallic: Excellent combination of strength and ductility, and unique microstructural features associated. *Acta Mater.* **2019**, *173*, 117–129. DOI:10.1016/j.actamat.2019.05.008
14. Wu ZQ, Huang CL, Xie LC, Hua L, Yuan YJ, Zhang LC. Machine learning assisted quality control in metal additive manufacturing: A review. *Adv. Powder Mater.* **2025**, *4*, 100342. DOI:10.1016/j.apmate.2025.100342
15. Chen Q, Zhao L, Xu LY, Han YD. Fabricating $Ti_2AlNb$-based high temperature alloy via electron beam powder bed fusion. *Mater. Today Commun.* **2025**, *48*, 113682. DOI:10.1016/j.mtcomm.2025.113682
16. Zhang SW, Xi M, Sun XX, Liu YY, Zheng C, Bai DM, et al. Significant effect of press down volume on microstructural evolution and mechanical properties of Ti2AlNb intermetallic alloy prepared by point-forging and laser-deposition. *Mater. Sci. Eng. A* **2024**, *907*, 146672. DOI:10.1016/j.msea.2024.146672
17. Zhang H, Zai L, Wang Y, Xue XH. Insight into microstructural evolution and mechanical property correlations of $Ti_2AlNb$-based alloy fabricated through wire arc additive manufacturing. *Mater. Sci. Eng. A* **2025**, *938*, 148477. DOI:10.1016/j.msea.2025.148477
18. Li ZX, Cui YN, Yu ZY, Liu CM. *In-situ* fabrication of $Ti_2AlNb$-based alloy through double-wire arc additive manufacturing. *J. Alloys Compd.* **2021**, *876*, 160021. DOI:10.1016/j.jallcom.2021.160021
19. Yu ZY, Li ZX, Guo YL, Fu R, Xu TQ, Liu CM. Homogenizing the composition of *in-situ* fabricated $Ti_2AlNb$-based alloy via manipulating the droplet transfer mode of twin-wire arc additive manufacturing. *J. Alloys Compd.* **2022**, *923*, 165992. DOI:10.1016/j.jallcom.2022.165992
20. Fu R, Yu ZY, Wu QR, Liu CM. Microstructure evolution and property strengthening of $Ti_2AlNb$ alloys prepared by multi-wire arc-directed energy deposition. *J. Mater. Process. Technol.* **2024**, *329*, 118460. DOI:10.1016/j.jmatprotec.2024.118460
21. Lei ZL, Zhang KZ, Zhou H, Ni LC, Chen YB. A comparative study of microstructure and tensile properties of $Ti_2AlNb$ joints prepared by laser welding and laser-additive welding with the addition of filler powder. *J. Mater. Process. Technol.* **2018**, *255*, 477–487. DOI:10.1016/j.jmatprotec.2017.12.044
22. Zhang YR, Liu YC, Yu LM, Liang HY, Huang Y, Ma ZQ. Microstructures and tensile properties of $Ti_2AlNb$ and Mo-modified $Ti_2AlNb$ alloys fabricated by hot isostatic pressing. *Mater. Sci. Eng. A* **2020**, *776*, 139043. DOI:10.1016/j.msea.2020.139043
23. Tang F, Nakazawa S, Hagiwara M. Effect of boron microalloying on microstructure, tensile properties and creep behavior of Ti–22Al–20Nb–2W alloy. *Mater. Sci. Eng. A* **2001**, *15*, 147–152. DOI:10.1016/S0921-5093(01)01155-8
24. Zhang PH, Zeng WD, Zhang F, Ma HY, Xu JW, Liang XB, et al. Fracture toughness of $Ti_2AlNb$ alloy with different Al content: Intrinsic mechanism, extrinsic mechanism and prediction model. *J. Alloys Compd.* **2023**, *952*, 170068. DOI:10.1016/j.jallcom.2023.170068
25. Germann L, Banerjee D, Guédou JY, Strudel JL. Effect of composition on the mechanical properties of newly developed $Ti_2AlNb$-based titanium aluminide. *Intermetallics* **2005**, *13*, 920–924. DOI:10.1016/j.intermet.2004.12.003
26. Zhang HY, Yan N, Liang HY, Liu YC. Phase transformation and microstructure control of $Ti_2AlNb$-based alloys: A review. *J. Mater. Sci. Technol.* **2021**, *80*, 203–216. DOI:10.1016/j.jmst.2020.11.022
27. Wei ZY, Miao BH, Shu SL, Yang HY, Zhong XM, Dong BX, et al. Opening the future of lightweight: Research progress in additive manufacturing of TiAl alloys. *J. Mater. Res. Technol.* **2025**, *39*, 5391–5414. DOI:10.1016/j.jmrt.2025.10.162
28. Chen YY, Shi GH, Du ZM, Zhang Y, Chang S. Research Progress on Additive Manufacturing TiAl Alloy. *Acta Metall. Sin.* **2024**, *60*, 1–15. DOI:10.11900/0412.1961.2022.00582 (In Chinese)
29. McCann R, Obeidi MA, Hughes C, McCarthy É, Egan DS, Vijayaraghavan RK, et al. *In-situ* sensing, process monitoring and machine control in Laser Powder Bed Fusion: A review. *Addit. Manuf.* **2021**, *45*, 102058. DOI:10.1016/j.addma.2021.102058
30. Wang H, Zhao L, Peng Y. Effects of laser power on microstructure and mechanical properties of TiAl-based alloys fabricated via laser melting deposition. *J. Mater. Res. Technol.* **2026**, *41*, 7309–7321. DOI:10.1016/j.jmrt.2026.02.153
31. Xue H, Song Y, Tong XH, Liang YF, Peng H, Wang YL, et al. Enhancing strength and ductility in high Nb-containing TiAl alloy additively manufactured via directed energy deposition. *Addit. Manuf.* **2024**, *86*, 104194. DOI:10.1016/j.addma.2024.104194
32. Thomas M, Malot T, Aubry P. Laser metal deposition of the intermetallic TiAl alloy. *Metall. Mater. Trans. A* **2017**, *48*, 3143. DOI:10.1007/s11661-017-4042-9

33. Liu Y, Hu K, Song J, Zheng X, Song Y, Bo S, et al. Crack formation mechanisms in laser-directed energy deposited high-Nb TiAl alloys. *Intermetallics* **2025**, *187*, 108975. DOI:10.1016/j.intermet.2025.108975
34. Bartlett JL, Li XD. An overview of residual stresses in metal powder bed fusion. *Addit. Manuf.* **2019**, *27*, 131–149. DOI:10.1016/j.addma.2019.02.020
35. Cao YD, Xing HZ, Li GS, Zhang SY, Li SC, Xu ZH, et al. Metal additive manufacturing: Processing, microstructures and mechanical properties. *Sci. Sin. Phys. Mech. Astron.* **2026**, *56*, 264614. DOI:10.1360/SSPMA-2025-0270 (In Chinese)
36. Liu YT, Zhang YZ. Microstructure and mechanical properties of TA15-$Ti_2AlNb$ bimetallic structures by laser additive manufacturing. *Mater. Sci. Eng. A* **2020**, *795*, 140019. DOI:10.1016/j.msea.2020.140019
37. Thompson SM, Bian L, Shamsaei N. An overview of Direct Laser Deposition for additive manufacturing; Part I: Transport phenomena, modeling and diagnostics. *Addit. Manuf.* **2015**, *8*, 36–62. DOI:10.1016/j.addma.2015.07.001
38. Yu GY, Dong Z, Chu X, Lu BW, Yan XC, Qiu H, et al. Microstructural characteristics and high-temperature hot corrosion behavior of TiAl alloy fabricated by electron beam melting. *J. Alloys Compd.* **2025**, *1038*, 182625. DOI:10.1016/j.jallcom.2025.182625
39. He WW, Chen QY, Tao H, Wang YF, Yuan XB, Zhang KJ, et al. Microstructure and tensile performance of an ultrafine-grained Ti–45Al–2Mn–2Nb–0.8vol% TiB2 alloy fabricated by selective electron beam melting. *J. Alloys. Compd.* **2026**, *1055*, 186467. DOI:10.1016/j.jallcom.2026.186467
40. Liu JH, Wang ZM, Li P, Zhang Z, Zhao CG, Zhao Y, et al. Fabrication of high strength TiAl alloy with nano-lamellar and ultra-fine-grained microstructure by selective electron beam melting. *J. Mater. Res. Technol.* **2025**, *35*, 7156–7166. DOI:10.1016/j.jmrt.2025.03.080
41. Xue XY, Bao JG, Wu ZK, Zhao Y, Da RH, Yang DB, et al. Additive manufacturing of $Ti_2AlNb$ alloys: A review of process, microstructure, property relationships. *Mater. Sci. Eng. R Rep.* **2026**, *169*, 101197. DOI:10.1016/j.mser.2026.101197
42. Gussone J, Rackel MW, Tumminello S, Barriobero-Vila P, Kreps F, Kelm K, et al. Microstructure formation during laser powder bed fusion of Ti–22Al–25Nb with low and high pre-heating temperatures. *Mater. Des.* **2023**, *232*, 112154. DOI:10.1016/j.matdes.2023.112154
43. Wang Y, Gao GF, Ming Z, Li RK, Ma WB, Xing DH, et al. Temperature-controlled ultrasonic vibration assisted machining response and improvement mechanism for $Ti_2AlNb$ alloy manufactured by directed energy deposition. *Chin. J. Aeronaut.* **2026**, 104091. DOI:10.1016/j.cja.2026.104091
44. Zhu ZH, Niu JZ, Zhang XZ, Liu N, Liang J, Wang J. Microstructure and mechanical behaviors of the additive-manufactured Ti–22Al–25Nb intermetallic fabricated via selective electron beam melting. *J. Alloys. Compd.* **2026**, *1061*, 187481. DOI:10.1016/j.jallcom.2026.187481
45. Wang GF, Yang YL, Jiao XY. Microstructure and mechanical properties of Ti–22Al–25Nb alloy fabricated by elemental powder metallurgy. *Mater. Sci. Eng. A* **2016**, *654*, 69–76. DOI:10.1016/j.msea.2015.12.037
46. Jia JB, Liu WC, Xu Y, Lu C, Liu HL, Gu YF, et al. Microstructure evolution, B2 grain growth kinetics and fracture behaviour of a powder metallurgy Ti–22Al–25Nb alloy fabricated by spark plasma sintering. *Mater. Sci. Eng. A* **2018**, *730*, 106–118. DOI:10.1016/j.msea.2018.05.110
47. Wang W, Zeng WD, Li D, Zhu B, Zheng YP, Liang XB. Microstructural evolution and tensile behavior of $Ti_2AlNb$ alloys based α2-phase decomposition. *Mater. Sci. Eng. A* **2016**, *662*, 120–128. DOI:10.1016/j.msea.2016.03.058
48. Wang W, Zeng WD, Liu YT, Xie GX, Liang XB. Microstructural evolution and mechanical properties of Ti–22Al–25Nb (at.%) orthorhombic alloy with three typical microstructures. *J. Mater. Eng. Perform.* **2018**, *27*, 293–303. DOI:10.1007/s11665-017-3040-9
49. Chen Q, Xu LY, Zhang YK, Zhao L, Hao KD, Ren WJ, et al. Additive manufacturing Ti–22Al–25Nb alloy with excellent high temperature tensile properties by electron beam powder bed fusion. *Addit. Manuf.* **2024**, *86*, 104236. DOI:10.1016/j.addma.2024.104236
50. Li HX, Che QY, He WW, Xiang CS, Cheng KK, Wang Y. Effect of heat treatment on microstructure and properties of $Ti_2AlNb$ alloy fabricated by selective electron beam melting. *Mater. China* **2023**, *42*, 499–505. DOI:10.7502/j.issn.1674-3962.202203024 (In Chinese)
51. Tang YJ, Liu YT, Zhang YZ. Effect of heat treatment on microstructure and properties of laser additive manufactured $Ti_2AlNb$-based alloy. *Aeronaut. Manuf. Technol.* **2016**, 16–21. DOI:10.16080/j.issn1671-833x.2016.19.016 (In Chinese)
52. Liu YT, Gong XY, Liu MK, Zhang YL. Microstructure and tensile properties of laser melting deposited $Ti_2AlNb$-based alloy. *Chin. J. Lasers* **2014**, *41*, 77–83. DOI:10.3788/CJL201441.0103005 (In Chinese)
53. Chen Q, Xu LY, Zhao L, Hao KD, Han YD. The effect of nitrogen on the tensile strength of Ti–22Al–25Nb alloy using laser beam powder bed fusion. *Mater. Sci. Eng. A* **2024**, *909*, 146815. DOI:10.1016/j.msea.2024.146815
54. Kang JM, Sun BB, Lu WQ, Qian M, Li JF. Cracking mechanisms in $Ti_2AlNb$ alloy fabricated by laser powder bed fusion. *J. Alloys Compd.* **2025**, *1036*, 181979. DOI:10.1016/j.jallcom.2025.181979

55. Yao XJ, Wang JW, Yang YC, Zhang XY, Chen X, Zhang SQ. Review on defect formation mechanisms and control methods of metallic components during laser additive manufacturing. *Chin. J. Lasers* **2022**, *49*, 1402802. DOI:10.3788/CJL202249.1402802
56. Chen Q, Xu LY, Zhao L, Hao KD, Han YD. Effect of scanning speed on microstructure and mechanical properties of as-printed Ti–22Al–25Nb intermetallic by laser powder bed fusion. *Mater. Sci. Eng. A* **2023**, *885*, 145652. DOI:10.1016/j.msea.2023.145652
57. Lopez A, Bacelar R, Pires I, Santos TG, Sousa JP, Quintino L. Non-destructive testing application of radiography and ultrasound for wire and arc additive manufacturing. *Addit. Manuf.* **2018**, *21*, 298–306. DOI:10.1016/j.addma.2018.03.020
58. Meng LX. Study on Defect Control and Mechanical Properties of Additively Manufactured Ti6Al4V Alloy. Ph.D. Thesis, University of Science and Technology of China, Hefei, China, 2024. DOI:10.27517/d.cnki.gzkju.2024.000032 (In Chinese)